



Article

# Memristor-Based Lozi Map with Hidden Hyperchaos

Jiang Wang, Yang Gu, Kang Rong, Quan Xu  and Xi Zhang \* 

School of Microelectronics and Control Engineering, Changzhou University, Changzhou 213164, China

\* Correspondence: zhangxi.98@163.com

**Abstract:** Recently, the application of memristors to improve chaos complexity in discrete chaotic systems has been paid more and more attention to. To enrich the application examples of discrete memristor-based chaotic systems, this article proposes a new three-dimensional (3-D) memristor-based Lozi map by introducing a discrete memristor into the original two-dimensional (2-D) Lozi map. The proposed map has no fixed points but can generate hidden hyperchaos, so it is a hidden hyperchaotic map. The dynamical effects of the discrete memristor on the memristor-based Lozi map and two types of coexisting hidden attractors boosted by the initial conditions are demonstrated using some numerical methods. The numerical results clearly show that the introduced discrete memristor allows the proposed map to have complicated hidden dynamics evolutions and also exhibit heterogeneous and homogeneous hidden multistability. Finally, a digital platform is used to realize the memristor-based Lozi map, and its experimental phase portraits are obtained to confirm the numerical ones.

**Keywords:** memristor-base Lozi map; discrete memristor; dynamical effect; hidden hyperchaos; multistability

MSC: 37E05



**Citation:** Wang, J.; Gu, Y.; Rong, K.; Xu, Q.; Zhang, X. Memristor-Based Lozi Map with Hidden Hyperchaos. *Mathematics* **2022**, *10*, 3426. <https://doi.org/10.3390/math10193426>

Academic Editors: Sajad Jafari, Kehui Sun and Bocheng Bao

Received: 29 August 2022

Accepted: 15 September 2022

Published: 21 September 2022

**Publisher's Note:** MDPI stays neutral with regard to jurisdictional claims in published maps and institutional affiliations.



**Copyright:** © 2022 by the authors. Licensee MDPI, Basel, Switzerland. This article is an open access article distributed under the terms and conditions of the Creative Commons Attribution (CC BY) license (<https://creativecommons.org/licenses/by/4.0/>).

## 1. Introduction

Because of the specific nonlinearity with an internal state [1], memristors have widely been used in plenty of continuous-time chaotic systems [2,3]. In general, the memristor-based continuous-time chaotic systems can exhibit complicated dynamics related to initial conditions, including various self-excited and hidden dynamical behaviors [4–9]. Thus, the memristor can provide the dynamical effect on the original chaotic system, which can make the memristor-based continuous-time chaotic system produce more complex dynamical behavior [10,11]. Nevertheless, the memristor-based discrete-time chaotic systems have not received much attention [12,13]. Therefore, it is interesting to effectively apply memristors to discrete-time chaotic systems and investigate the complicated dynamics of the newly constructed discrete-time systems.

Distinguishing them from the common self-excited attractors, special hidden attractors are a class of attractors whose basins of attraction are not associated with the neighborhoods of unstable equilibria [14,15]. Since the discovery of the special hidden attractors, many continuous-time hidden chaotic systems with only stable equilibria or no equilibria have been thereby proposed [16–22]. In contrast, discrete-time chaotic systems belong to a special kind of dynamical systems that use discrete-time variables to describe the instantaneous states. Recently, such special hidden strange attractors have also been found in discrete-time chaotic systems of the Vertigo map [23], sine hyperchaotic map [24], quadratic chaotic map [25], fractional-order map [26], and polynomial map [27]. In particular, discrete-time fractional-order systems can also exhibit rich dynamical behaviors, including chaos and projective synchronization [28], as well as period-doubling, Hopf, and symmetry-breaking bifurcations [29]. Therefore, how to construct discrete-time chaotic systems and study the bifurcation mechanism of the hidden attractors has been paid close attention by researchers.

As a specific nonlinearity with the internal state, a memristor can also be used to build various discrete-time chaotic systems, and it can bring very rich dynamical effects to the original systems. In recent years, some novel memristor-based discrete-time chaotic systems have been proposed through the discrete-time modeling of memristors [30–34]. According to Euler’s difference algorithm, a discrete-time memristor model was designed, and a memristive Hénon chaotic map was proposed [30]. By establishing a unified discrete-time memristor mapping model, four novel memristive hyperchaotic maps were directly derived [31]. By leading a discrete-time memristor model to the original Sine-type map, a new memristor-based hyperchaotic map was established, and its dynamical mechanism was thereby explored [32]. Moreover, by employing a discrete-time memristor to characterize the magnetic induction effect, a memristive Rulkov neuron model was implemented, and its complicated regime transitions and hyperchaotic firings were uncovered therein [13]. As a result, modeling and analysis of memristor-based discrete-time maps have gradually become a new research topic, which has significant theoretical and application values [35,36].

Inspired by the above research idea, this article proposes a new 3-D memristor-based Lozi map with hidden hyperchaos through coupling a discrete memristor into the original Lozi map, which is expected to enrich the application examples of discrete-time memristor-based chaotic systems. The remainder of the article is organized as follows. In Section 2, a new memristor-based Lozi map with no fixed points is proposed. In Section 3, the dynamical effect of the memristor on the memristor-based Lozi map is investigated. Heterogeneous hidden multistability and homogeneous hidden multistability are disclosed in Section 4, and the experimental phase portraits are obtained to confirm the numerical ones in Section 5. The last section concludes this article.

## 2. Modeling of Memristor-Based Lozi Map

In this section, a new 3-D memristor-based Lozi map is established by coupling a discrete memristor to the original 2-D Lozi map. Since there are no fixed points but hyperchaos can emerge, the memristor-based Lozi map is a hidden hyperchaotic map.

### 2.1. Brief Review of the Lozi Map

The original Lozi map is a 2-D discrete-time chaotic system [37], and its mathematical model is written as

$$\begin{cases} x_{n+1} = 1 - a|x_n| + y_n, \\ y_{n+1} = bx_n, \end{cases} \quad (1)$$

where  $x, y$  are two state variables, and  $a, b$  are two real-valued control parameters.

When the two control parameters change in  $a \in [1, 2]$  and  $b \in [-1.1, 0.9]$ , the 2-D hybrid bifurcation plot of the 2-D Lozi map is shown in Figure 1a, which contains multiple bounded behavior regions in multiple colors and an unbounded behavior (UB) region in gray. Note that a detailed description of the 2-D hybrid bifurcation plot is given in the following section. The bounded behaviors mainly include chaos (CH) in magenta, stable point (P0) in brown, and period-2 (P2) in black. More interestingly, there are two boundary lines between the chaos region and the period-2 region as well as between the chaos region and the stable point region, indicating that chaos is caused by the border-collision bifurcation, which is consistent with the bifurcation mechanism of the route to chaos in most switching converters [38]. For the representative values  $(a, b) = (1.7, 0.5)$ , the Lozi map has two fixed points and can generate a strange attractor. The typical strange attractor with V-shaped structure is shown in Figure 1b. Therefore, the 2-D Lozi map has a border-collision bifurcation route to chaos, but only exhibits a simple dynamics distribution with self-excited oscillation patterns.

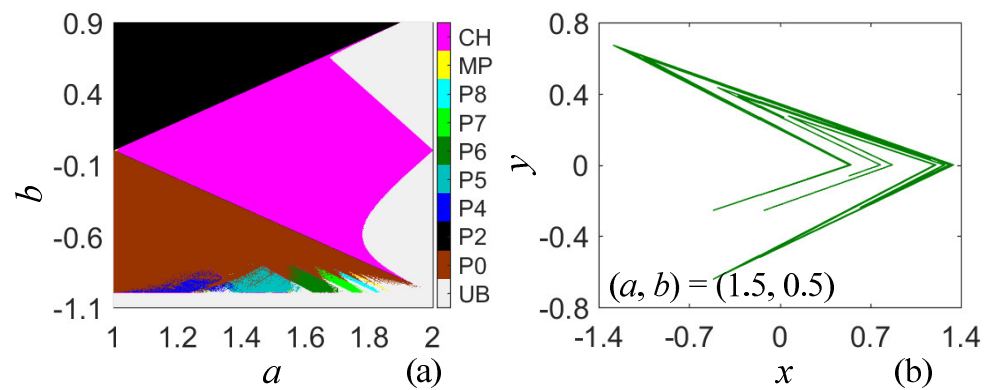


**Figure 1.** For fixed  $(x_0, y_0, z_0) = (0, 0, 0)$ , (a) the 2-D hybrid bifurcation plot and (b) typical strange attractor of the 2-D Lozi map.

### 2.2. Discrete-Time Modeling of Memristor

For the input current  $i(t)$  and the terminal voltage  $v(t)$ , a charge-controlled ideal memristor can be modeled as

$$\begin{aligned} v(t) &= M(q) \cdot i(t) = \sin q(t) \cdot i(t), \\ dq(t)/dt &= i(t), \end{aligned} \tag{2}$$

where  $q$  is the charge variable and  $M(q) = \sin q(t)$  is the memristance function. The continuous-time model of the memristor described by (2) can show the pinched hysteresis loops that rely on the stimulus frequencies and memristor initial states when the continuous-time sine currents are applied.

Let  $i_n, v_n$ , and  $q_n$  be the sampled values of  $i(t), v(t)$ , and  $q(t)$  at the  $n$ -th iteration, and  $q_{n+1}$  be the sampled value of  $q(t)$  at the  $(n + 1)$ -th iteration. Based on the continuous-time memristor model in (2), a discrete-time memristor model can be mathematically described by referring to [31] as

$$\begin{aligned} v_n &= M(q_n)i_n = \sin(q_n)i_n, \\ q_{n+1} &= q_n + hi_n, \end{aligned} \tag{3}$$

where  $M(q_n) = \sin(q_n)$  and  $h$  is specified as 1. Similar to the continuous-time memristor model, the discrete-time memristor model can also exhibit pinched hysteresis loops when the discrete-time sine currents are applied [31].

### 2.3. Memristor-Based Lozi Map with no Fixed Points

To promote the chaos complexity of the Lozi map, a new 3-D memristor-based Lozi map is proposed by coupling the discrete-time memristor given in (3) into the original Lozi map described by (1). For the discrete memristor, the state variable  $y_n$  in the Lozi map is denoted as the input, and the state variable  $z_n$  is denoted as the internal state. Then the output of the discrete memristor becomes  $v_n = y_n \sin z_n$ , which is coupled to the second equation of the Lozi map after the gain  $k$ . Therefore, the memristor-based Lozi map can be constructed as

$$\begin{cases} x_{n+1} = 1 - a|x_n| + y_n, \\ y_{n+1} = bx_n + ky_n \sin z_n, \\ z_{n+1} = y_n + z_n, \end{cases} \tag{4}$$

where  $k$  is the coupling gain between the discrete-time memristor and the Lozi map.

Let  $P = (X, Y, Z)$  be a fixed point of the memristor-based Lozi map. The fixed point  $P$  should satisfy the following algebraic equations

$$\begin{cases} X = 1 - a|X| + Y, \\ Y = bX + kY \sin Z, \\ Z = Y + Z. \end{cases} \tag{5}$$

By solving (5), we obtain  $Y = 0$  from the third equation, and then substitute  $Y = 0$  into the second equation to deduce  $X = 0$ . However, when  $X = 0$  and  $Y = 0$  are substituted into the first equation, there is no solution to the first equation, implying that  $P = (X, Y, Z)$  is not a solution to (5). Therefore, the memristor-based Lozi map has no fixed points, showing that its dynamical behaviors are all hidden when bounded iterations occur. In other words, the memristor-based Lozi map is a specific hidden discrete-time system.

To calculate the Lyapunov exponents (LEs) of the memristor-based Lozi map, the Jacobian matrix can be yielded by deriving the partial derivatives from (4) as

$$\mathbf{J} = \begin{bmatrix} -a \operatorname{sgn}(x_n) & 1 & 0 \\ b & k \sin z_n & ky_n \cos z_n \\ 0 & 1 & 1 \end{bmatrix}. \quad (6)$$

Because there are no fixed points, the Jacobian matrix in (6) cannot be used to evaluate the stability of the memristor-based Lozi map and can only be applied to the LE calculation based on Wolf's algorithm [31].

### 3. Dynamical Effect Induced by Discrete Memristor

In this section, the dynamical effect of memristor on the 3-D memristor-based Lozi map is investigated using 2-D hybrid bifurcation plots, one-dimensional (1-D) bifurcation plots, and phase portraits.

#### 3.1. 2-D Hybrid Bifurcation Plots

By detecting the iteration periods and LEs of the iterative sequences generated by the proposed memristor-based Lozi map, the colorful 2-D hybrid bifurcation plot can be employed to show the dynamical effect of the discrete memristor on the memristor-based Lozi map. Here, we set the initial conditions as  $(x_0, y_0, z_0) = (0, 0, 0)$  and the two control parameters  $a, b$  are utilized to construct the 2-D parameter plane and select the interception interval of the iteration sequence as  $[10^5, 10^5 + 100]$ . For each set of parameters in the 2-D hybrid bifurcation plot, the memristor-based Lozi map generates an iterative sequence with a certain dynamical behavior. The parameter regions corresponding to the iterative sequences with different dynamical behaviors are colored differently. Note that Wolf's Jacobian numerical method with the iteration length  $2 \times 10^5$  is utilized to calculate the three LEs [31].

For four determined values of  $k$ , the 2-D hybrid bifurcation plots are shown in Figure 2, where the adjustable ranges of the two control parameters are unified as  $a \in [-1, 1.6]$  and  $b \in [-0.8, 0.4]$ . The red blocks (labeled as HC) correspond to the hidden hyperchaotic behaviors of two positive LEs, the magenta blocks (labeled as CH) correspond to the hidden chaotic behaviors of one positive LE, the yellow blocks (labeled as MP) correspond to the hidden periodic behaviors of a period over 8 and no positive LEs, and the other color blocks (labeled as P2, P3, up to P8) correspond to the hidden period-2, to hidden period-3, up to hidden period-8 behaviors of no positive LEs. Besides, the gray blocks (labeled as UB) correspond to the unbounded behavior. Consequently, the memristor-based Lozi map has complicated hidden dynamics distributions in the plane of two control parameters, including hidden hyperchaos, hidden chaos, hidden multi-period, hidden period, and unbounded behavior. As can be seen, the 2-D hybrid bifurcation plots in Figure 2 effectively manifest the dynamical effects of the memristor on the proposed memristor-based Lozi map, i.e., the discrete memristor can enhance the complexity of the dynamic distribution of the original Lozi map.

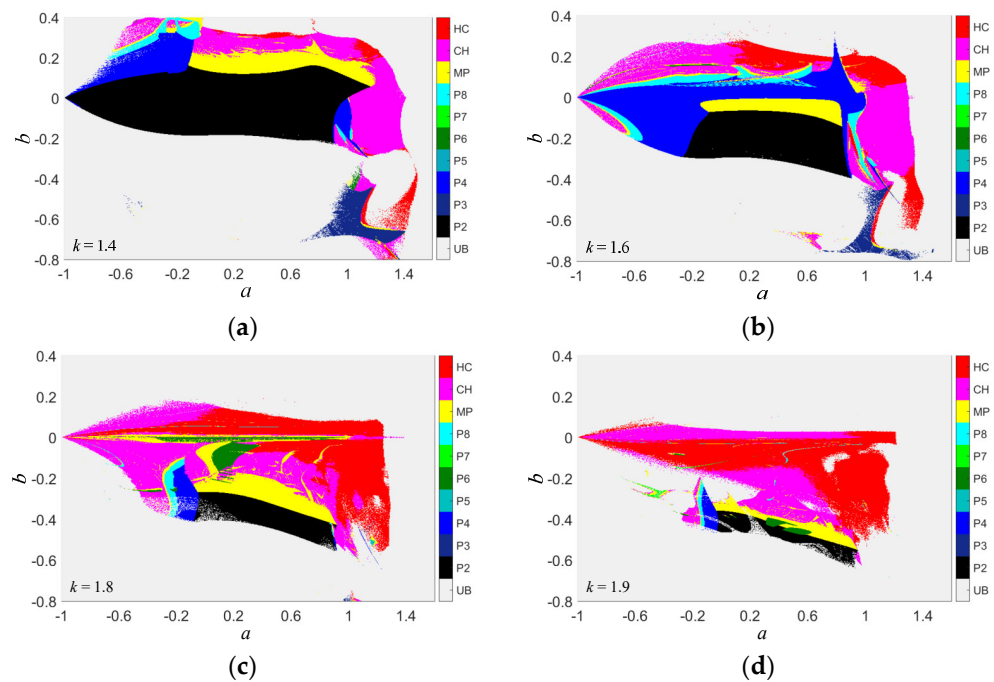


**Figure 2.** For the initial conditions  $(x_0, y_0, z_0) = (0, 0, 0)$ , the 2-D hybrid bifurcation plot of the memristor-based Lozi map at four determined values of  $k$ : (a)  $k = 1.4$ ; (b)  $k = 1.6$ ; (c)  $k = 1.8$ ; (d)  $k = 1.9$ .

The hidden dynamical distributions of the 2-D hybrid bifurcation plots in Figure 2 consist of the hidden bounded behavior regions in plenty of colors and the unbounded behavior (UB) region in gray. The hidden bounded behaviors mainly include hidden chaos (CH) in magenta, hidden hyperchaos (HC) in red, hidden period-2 (P2) in black, hidden period-4 (P4) in blue, and hidden multi-period in yellow, and these hidden bounded behaviors have relatively large dynamics distribution regions. However, the hidden bounded behaviors of other hidden period-3 (P3), period-5 (P5), period-6 (P6), period-7 (P7), and period-8 (P8) have relatively small dynamic distribution regions. By contrast, as shown in Figure 2a, when  $k = 1.4$ , the hidden chaos and period-2 behaviors have large distribution regions. As shown in Figure 2b, when  $k = 1.6$ , the distribution region of hidden period-2 behavior is reduced, while the distribution regions of hidden hyperchaos and period-4 behaviors are increased. As shown in Figure 2c,d, when  $k = 1.8$  and  $1.9$ , i.e., as  $k$  increases further, the distribution region of hidden hyperchaos behavior further increases, while the distribution regions of other hidden chaos and period behaviors become smaller and smaller. Therefore, these results in Figure 2 clarify that the discrete memristor indeed has complicated dynamical effects on the memristor-based Lozi map.

### 3.2. 1-D Bifurcation Plots and Hidden Hyperchaos

The 1-D bifurcation plots consist of bifurcation diagrams and corresponding LE spectra, which can be employed to investigate the bifurcation behaviors of the 3-D memristor-based Lozi map. According to the 2-D hybrid bifurcation plot in Figure 2c, we determine that the two control parameters  $b$  and  $k$  are unchanged and the model parameter  $a$  is changeable. When fixing  $b = -0.1$ ,  $k = 1.8$ , and varying  $a$  in the region  $[-0.7, 1.2]$ , the bifurcation diagrams of state variables  $x, y$  (bottom) and corresponding LE spectra (top) are numerically depicted in Figure 2a. As the evolution of  $a$ , the memristor-based Lozi map can display hidden hyperchaos with two positive LEs, hidden chaos with one positive LE, and hidden period-6 and period-12 with negative first LE, as well as several hidden periodic windows.

Observed from Figure 2, the discrete memristor has complicated dynamical effects on the memristor-based Lozi map. In other words, the hidden bifurcation behaviors of the memristor-based Lozi map are dependent on the coupling gain  $k$ . Similarly, when fixing  $a = 1$ ,  $b = -0.1$ , and varying  $k$  in the region  $[1.4, 1.9]$ , the bifurcation diagrams of state

variables  $x, y$  (bottom) and the LE spectra (top) are numerically plotted in Figure 3b. With the increase in  $k$ , the memristor-based Lozi map only displays hidden hyperchaos with two positive LEs, hidden chaos with one positive LE, and hidden period-4 and period-8 with negative first LE. In particular, the hidden chaotic and hidden hyperchaotic behaviors are robust to the coupling gain  $k$ . Besides, when  $k = 1.54$ , a fantastic route to chaos via hidden border-collision bifurcation can be found in the memristor-based Lozi map.

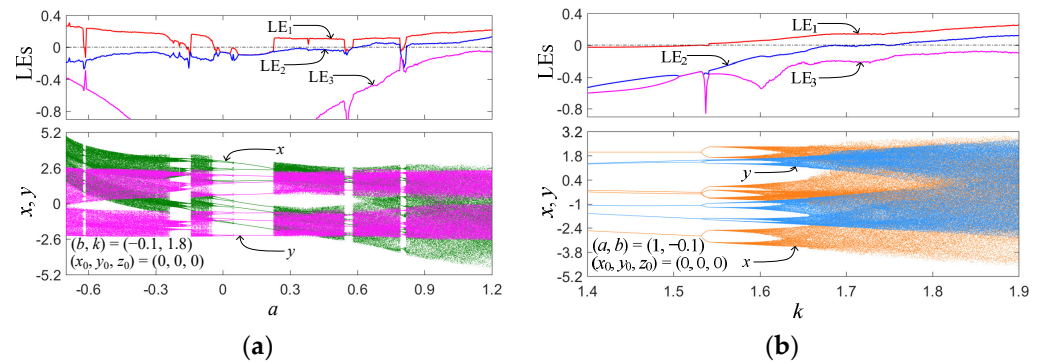


**Figure 3.** For the initial conditions  $(x_0, y_0, z_0) = (0, 0, 0)$ , the 1-D bifurcation plots consisting of bifurcation diagrams of state variables  $x, y$  (bottom) and corresponding LE spectra (top) as the two control parameters  $a, k$  vary in their respective regions: (a)  $a \in [-0.7, 1.2]$  with fixed  $b = -0.1$  and  $k = 1.8$ ; (b)  $k \in [1.4, 1.9]$  with fixed  $a = 1$  and  $b = -0.1$ .

With the simulated results in Figures 2 and 3, four groups of control parameters are determined to reveal the hidden hyperchaotic attractors generated by the memristor-based Lozi map. For the initial conditions  $(x_0, y_0, z_0) = (0, 0, 0)$ , the phase portraits projected on the  $x-z$  plane are simulated, and the numerical results are displayed in Figure 4, in which the iteration length is  $2 \times 10^5$ . In addition, we also determine the first two LEs ( $LE_1$  and  $LE_2$ ) and list the calculation results in Table 1. As can be found, all four hidden hyperchaotic attractors with two positive LEs have different and particularly complicated fractal structures, while the original 2-D Lozi map only has simple chaotic attractor structures. In brief, the discrete memristor can greatly enhance the fractal structure complexity of the strange attractor in the original 2-D Lozi map.

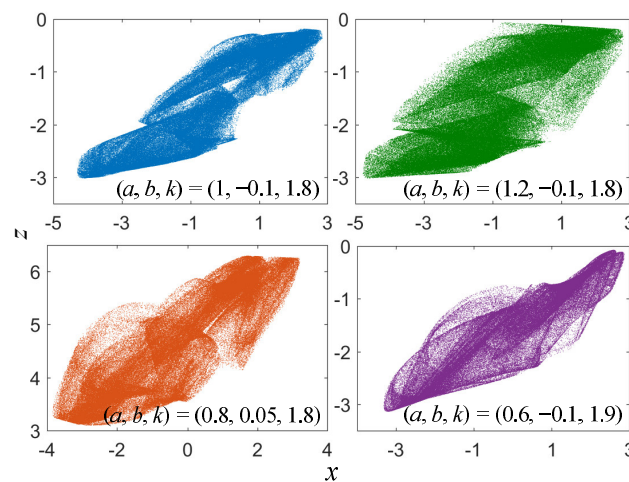


**Figure 4.** For four groups of control parameters with  $(x_0, y_0, z_0) = (0, 0, 0)$ , the phase portraits (in the  $x-z$  plane) of the hidden hyperchaotic attractors generated by the memristor-based Lozi map. The four groups of control parameters  $(a, b, k)$  are provided in the images.

**Table 1.** Performance evolutions for hidden hyperchaotic attractors under different control parameters.

$a, b, k$	$(LE_1, LE_2)$	PermEn	CorDim	$D_{KY}$
1, -1, 1.8	0.1811, 0.0522	4.0498	1.9578	3.0000
1.2, -0.1, 1.8	0.2174, 0.1286	4.2544	1.9900	3.0000
0.8, 0.05, 1.8	0.2232, 0.1159	4.1908	2.0036	3.0000
0.6, -0.1, 1.9	0.2531, 0.0342	3.8748	1.8348	2.5450

Moreover, similar to the performance analyses given in [36], the performance of the four hidden hyperchaotic attractors shown in Figure 4 is evaluated by employing the main performance indicators such as permutation entropy (PermEn), the correlation dimension (CorDim), and the Kaplan–Yorke dimension ( $D_{KY}$ ). The calculation results of these performance indicators are listed in Table 1. Meanwhile, the performance indicators of the typical chaotic attractor generated by the 2-D Lozi map in Figure 4 (right) are  $(LE_1, LE_2) = (0.4701, -1.1632)$ , PermEn = 3.8410, CorDim = 1.3915, and  $D_{KY} = 1.4041$ . Consequently, all the hidden hyperchaotic attractors shown in Figure 4 have excellent performance indicators, further indicating that the discrete memristor is feasible to promote the chaos complexity of the original 2-D Lozi map.

#### 4. Heterogeneous and Homogeneous Hidden Multistability

In this section, two types of coexisting hidden attractors boosted by the initial conditions, i.e., heterogeneous and homogeneous hidden multistability, are disclosed in the 3-D memristor-based Lozi map using basins of attraction and phase portraits.

##### 4.1. Coexistence of Heterogeneous Hidden Attractors

Multistability is an inherent property often encountered in chaotic systems [39], which can be manifested as the coexisting behavior of multiple attractors in the space of initial conditions. When multistability occurs, the long-term dynamical behaviors of the chaotic system are greatly influenced by the initial conditions in the respective regions of attraction. For some specific control parameters, the 3-D memristor-based Lozi map can show heterogeneous and homogeneous hidden multistability. It should be noted that heterogeneous hidden multistability implies the coexisting behavior of multiple hidden attractors of different stability types, while homogeneous hidden multistability indicates the coexisting behavior of multiple hidden attractors of the same stability type but only in different dynamic intervals.

The basin of attraction can be employed to classify the long-term coexisting behaviors of multiple hidden attractors by marking different regions on the plane of initial conditions with different colors. Two groups of control parameters  $(a, b, k)$  are determined as  $(1, 0.2, 1.37)$  and  $(1, 0.2, 1.4)$ . Thus, the basins of attraction are plotted in the  $x_0-z_0$  plane with  $y_0 = 0$ , as shown in Figure 5(a1,b1). The magenta, dark-green, red, and yellow regions stand for chaos (CH), period-6 (P6), hyperchaos (HC), and multi-period (MP), respectively. As can be revealed, the heterogeneous hidden bi-stability phenomena of the coexisting hidden attractors can be demonstrated in the 3-D memristor-based Lozi map.

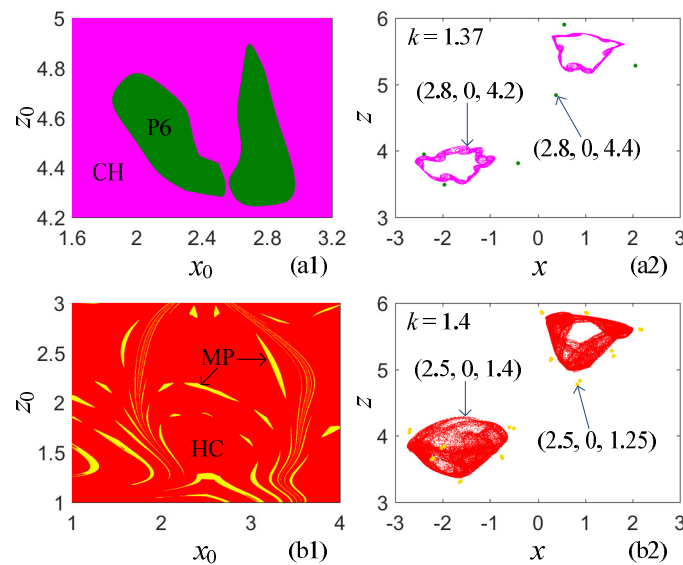


**Figure 5.** Coexisting behaviors of heterogeneous hidden attractors in the 3-D memristor-based Lozi map for two groups of control parameters, (a1,b1) are the basins of attraction in the  $x_0$ - $z_0$  plane with  $y_0 = 0$ , and (a2,b2) are the phase portraits in the  $x$ - $z$  plane: (a) Coexistence of hidden chaotic and period-6 attractors at  $(a, b, k) = (1, 0.2, 1.37)$ ; (b) coexistence of hidden hyperchaotic and multi-periodic attractors at  $(a, b, k) = (1, 0.2, 1.4)$ .

In addition, the coexisting heterogeneous hidden attractors under two groups of initial conditions are disclosed and their phase portraits in the  $x$ - $z$  plane are shown in Figure 5(a2,b2). The initial conditions of the chaotic and period-6 hidden attractors in Figure 5(a2) are picked from the magenta and dark-green regions in Figure 5(a1), whereas those of the hyperchaotic and multi-period hidden attractors in Figure 5(b2) are obtained from the red and yellow regions in Figure 5(b1). The numerical results effectively verify the appearance of heterogeneous hidden bi-stability in the 3-D memristor-based Lozi map.

#### 4.2. Coexistence of Homogeneous Hidden Hyperchaotic Attractors

In addition to the coexistence of heterogeneous hidden attractors mentioned above, the memristor-based Lozi map is most likely to produce the coexistence of homogeneous hidden hyperchaotic attractors, i.e., homogeneous hidden multistability.

We take the control parameters  $(a, b, k) = (1, -0.1, 1.8)$  as an example. To exhibit the long-term dynamical behaviors of each set of initial conditions in the 3-D memristor-based Lozi map, the basin of attraction in the  $x_0$ - $z_0$  plane with  $y_0 = 0$  is depicted in Figure 6a, where the variable ranges of initial conditions on the horizontal and vertical axes are  $x_0 \in [-4, 6]$  and  $z_0 \in [-16, 16]$ , respectively. The attractive regions of hidden hyperchaotic attractors with different dynamic intervals are perfectly homogeneous, and there are several fractal boundaries that clearly divide these attractive regions. Note that the iteration trajectories starting from each color region in the basin of attraction given in Figure 6a tend to be a hidden hyperchaotic attractor in the same dynamic interval.



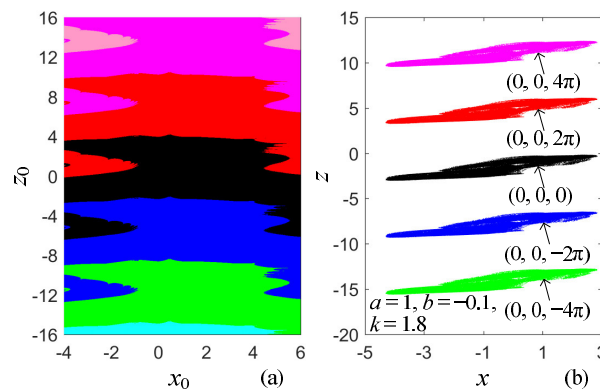


**Figure 6.** For  $(a, b, k) = (1, -0.1, 1.8)$  and  $y_0 = 0$ , **(a)** the basin of attraction within  $x_0 \in [-4, 6]$  and  $z_0 \in [-16, 16]$  and **(b)** the phase portrait of homogeneous hidden hyperchaotic attractors boosted by memristor initial condition.

The first two initial conditions are set to  $(x_0, y_0) = (0, 0)$  and the third initial condition, i.e., memristor initial condition, is assigned as  $z_0 = 2m\pi$  ( $m = -2, -1, 0, 1, 2$ ). Correspondingly, five homogeneous hidden hyperchaotic attractors with different dynamic intervals can be generated in the 3-D memristor-based Lozi map, and their phase portrait in the  $x$ - $z$  plane is shown in Figure 6b. The numerical results show that the dynamic intervals of the homogeneous hidden hyperchaotic attractors can be controlled regularly by the memristor initial conditions with a period of  $2\pi$  along the  $z$ -axis.

The same performance indicators listed in Table 1 are used to evaluate the performance of the homogeneous hidden hyperchaotic attractors controlled by the memristor initial conditions. Corresponding to the homogeneous hidden hyperchaotic attractors in Figure 6b, the performance indicators, such as  $LE_1$ ,  $LE_2$ , PermEn, CorDim, and  $D_{KY}$ , are listed in Table 2. Thus, these homogeneous hidden hyperchaotic attractors have almost identical calculation values. The small differences are mainly brought by unavoidable calculation errors. Therefore, the homogeneous hidden hyperchaotic attractors from the 3-D memristor-based Lozi map can be robustly controlled by the memristor’s initial conditions.

**Table 2.** Performance evolutions for homogeneous hidden hyperchaotic attractors under different memristor initial conditions.

$z_0 = 2m\pi$	$(LE_1, LE_2)$	PermEn	CorDim	$D_{KY}$
$z_0 = 4\pi$	0.1800, 0.0508	4.0513	1.9495	3.0000
$z_0 = 2\pi$	0.1805, 0.0493	4.0467	1.9629	3.0000
$z_0 = 0$	0.1811, 0.0522	4.0498	1.9578	3.0000
$z_0 = -2\pi$	0.1803, 0.0521	4.0431	1.9501	3.0000
$z_0 = -4\pi$	0.1813, 0.0498	4.0543	1.9791	3.0000

### 5. Microcontroller-Based Hardware Experiments

Based on a high-performance microcontroller, we can implement the 3-D memristor-based Lozi map in a digital circuit. Thus, the generated hidden hyperchaotic attractors can be physically obtained by a digital oscilloscope.

The STM32F407 family chip is considered the selected microcontroller. The experimental platform mainly includes a 32-bit STM32F407VET6 microcontroller, a 16-bit DAC8563 D/A converter, and an interface circuit. The microcontroller is used to implement the memristor-based Lozi map, and the D/A converter provides the analog voltage output. The run program with the control parameter and initial condition settings is coded using C language and uploaded to the microcontroller.

The control parameter and initial condition settings are the same as those given in Figures 4–6. Utilizing the experiment platform for the numerical phase portraits in Figure 4,

the experimental phase portraits of the four hidden hyperchaotic attractors are captured on a digital oscilloscope, as shown in Figure 7. Similarly, for the numerical phase portraits in Figures 5 and 6, the experimental phase portraits of the coexisting heterogeneous hidden attractors and coexisting homogeneous hidden hyperchaotic attractors are obtained by a digital oscilloscope, as shown in Figure 8. In the captured figures, the Ch1 and Ch2 labels denote the  $x$ -axis and  $y$ -axis channels, respectively. The experimental phase portraits validate the numerical phase portraits, indicating the feasibility of the hardware experiment platform for the implementation of the 3-D memristor-based Lozi map.

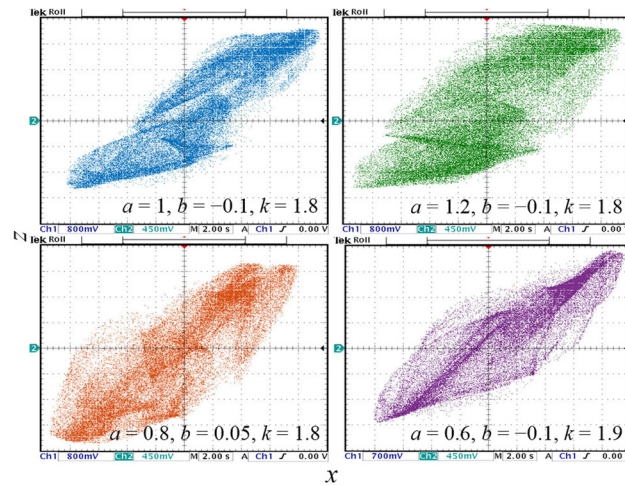


**Figure 7.** Corresponding to the numerical results in Figure 4, the experimental phase portraits of the four hidden hyperchaotic attractors. The four groups of control parameters  $(a, b, k)$  are provided in the images.

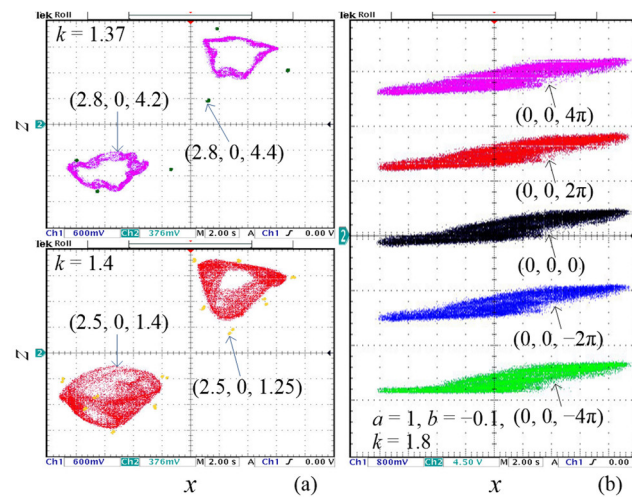


**Figure 8.** The experimental phase portraits corresponding to the numerical ones in Figures 5 and 6, where the control parameter and initial condition settings are provided in the images: (a) Coexisting heterogeneous hidden attractors; (b) coexisting homogeneous hidden hyperchaotic attractors.

### 6. Conclusions

In this article, a new 3-D memristor-based Lozi map with hidden hyperchaos was proposed by coupling a discrete memristor to the original 2-D Lozi map [37], which is expected to enrich the application examples of discrete-time memristor-based chaotic systems. The proposed map has no fixed points, but can produce hyperchaos, so it is a special hidden hyperchaotic map. By employing some numerical methods, the dynamical effects of the discrete memristor on the memristor-based Lozi map and two types of coexisting hidden

attractors boosted by the initial conditions were clearly demonstrated. The numerical results showed that the discrete memristor allows the proposed map to have complicated hidden dynamics evolutions and to also exhibit heterogeneous and homogeneous hidden multistability. Finally, a digital platform was exploited, and its experimental phase portraits were obtained to confirm the numerical ones. Of course, the method to realize the applications of such a hidden hyperchaotic map in chaos-based secure communication [12] and generative adversarial nets [40] remains to be studied in the future.

**Author Contributions:** Data curation, Y.G.; Supervision, X.Z.; Visualization, K.R.; Writing—original draft, J.W.; Writing—review & editing, Q.X. All authors have read and agreed to the published version of the manuscript.

**Funding:** This research was supported by grants from the National Natural Science Foundation of China under Grant No. 12172066, and the Scientific Research Foundation of Jiangsu Provincial Education Department, China, under Grant No. 22KJB510001.

**Institutional Review Board Statement:** Not applicable.

**Informed Consent Statement:** Not applicable.

**Data Availability Statement:** Data generated during the current study will be made available at reasonable request.

**Conflicts of Interest:** The authors declare that they have no conflict of interest.

## References

- Chua, L.O. The fourth element. *Proc. IEEE* **2012**, *100*, 1920–1927. [CrossRef]
- Zhang, G.; Ma, J.; Alsaedi, A.; Ahmad, B.; Alzahrani, F. Dynamical behavior and application in Josephson Junction coupled by memristor. *Appl. Math. Comput.* **2018**, *321*, 290–299. [CrossRef]
- Chen, M.; Sun, M.X.; Bao, H.; Hu, Y.H.; Bao, B.C. Flux-charge analysis of two-memristor-based Chua’s circuit: Dimensionality decreasing model for detecting extreme multistability. *IEEE Trans. Ind. Electron.* **2020**, *67*, 2197–2206. [CrossRef]
- Fonzin, T.F.; Srinivasan, K.; Kengne, J.; Pelap, F.B. Coexisting bifurcations in a memristive hyperchaotic oscillator. *AEÜ Int. J. Electron. Commun.* **2018**, *90*, 110–122. [CrossRef]
- Min, F.H.; Li, C.; Zhang, L.; Li, C.B. Initial value-related dynamical analysis of the memristor-based system with reduced dimensions and its chaotic synchronization via adaptive sliding mode control method. *Chin. J. Phys.* **2019**, *58*, 117–131. [CrossRef]
- Volos, C.K.; Akgul, A.; Pham, V.T.; Baptista, M.S. Antimonotonicity, crisis and multiple attractors in a simple memristive circuit. *Circuits Syst. J. Comput.* **2018**, *27*, 1850026. [CrossRef]
- Njitacke, Z.T.; Kengne, J.; Tapche, R.W.; Pelap, F.B. Uncertain destination dynamics of a novel memristive 4D autonomous system. *Chaos Solitons Fractals* **2018**, *107*, 177–185. [CrossRef]
- Chen, C.J.; Bao, H.; Chen, M.; Xu, Q.; Bao, B.C. Non-ideal memristor synapse-coupled bi-neuron Hopfield neural network: Numerical simulations and breadboard experiments. *AEÜ Int. J. Electron. Commun.* **2019**, *94*, 26–35. [CrossRef]
- Ramamoorthy, R.; Rajagopal, K.; Leutcho, G.D.; Krejcar, O.; Namazi, H.; Hussain, I. Multistable dynamics and control of a new 4D memristive chaotic Sprott B system. *Chaos Solitons Fractals* **2022**, *156*, 111834. [CrossRef]
- Bao, H.; Ding, R.Y.; Hua, M.J.; Bao, B.C.; Chen, B. Incremental integral reconstitution for detecting initial condition effects. *AEÜ Int. J. Electron. Commun.* **2022**, *149*, 154178. [CrossRef]
- Mezatio, B.A.; Motchongom, M.T.; Tekam, B.R.W.; Kengne, R.; Tchitnga, R.; Fomethe, A. A novel memristive 6D hyperchaotic autonomous system with hidden extreme multistability. *Chaos Solitons Fractals* **2019**, *120*, 100–115. [CrossRef]
- Li, H.Z.; Hua, Z.Y.; Bao, H.; Zhu, L.; Chen, M.; Bao, B.C. Two-dimensional memristive hyperchaotic maps and application in secure communication. *IEEE Trans. Ind. Electron.* **2021**, *68*, 9931–9940. [CrossRef]
- Li, K.X.; Bao, H.; Li, H.Z.; Ma, J.; Hua, Z.Y.; Bao, B.C. Memristive Rulkov neuron model with magnetic induction effects. *IEEE Trans. Ind. Inform.* **2022**, *18*, 1726–1736. [CrossRef]
- Dudkowski, D.; Jafari, S.; Kapitaniak, T.; Kuznetsov, N.V.; Leonov, G.A.; Prasad, A. Hidden attractors in dynamical systems. *Phys. Rep.* **2016**, *637*, 1–50. [CrossRef]
- Wang, N.; Zhang, G.S.; Kuznetsov, N.V.; Bao, H. Hidden attractors and multistability in a modified Chua’s circuit. *Commun. Nonlinear Sci. Numer. Simul.* **2021**, *92*, 105494. [CrossRef]
- Doubla, I.S.; Ramakrishnan, B.; Njitacke, Z.T.; Kengne, J.; Rajagopal, K. Hidden extreme multistability and its control with selection of a desired attractor in a non-autonomous Hopfield neuron. *AEÜ Int. J. Electron. Commun.* **2022**, *144*, 154059. [CrossRef]
- Rajagopal, K.; Bayani, A.; Khalaf, A.J.M.; Namazi, H.; Jafari, S.; Pham, V.T. A no-equilibrium memristive system with four-wing hyperchaotic attractor. *AEÜ Int. J. Electron. Commun.* **2018**, *95*, 207–215. [CrossRef]
- Bao, H.; Hu, A.H.; Liu, W.B.; Bao, B.C. Hidden bursting firings and bifurcation mechanisms in memristive neuron model with threshold electromagnetic induction. *IEEE Trans. Neural. Netw. Learn. Syst.* **2020**, *31*, 502–511. [CrossRef]

19. Zhang, S.; Zeng, Y.C.; Li, Z.J.; Zhou, C.Y. Hidden extreme multistability, antimonotonicity and offset boosting control in a novel fractional-order hyperchaotic system without equilibrium. *Int. J. Bifurc. Chaos* **2018**, *28*, 1850167. [[CrossRef](#)]
20. Marius, F.D.; Michal, F. Hidden chaotic attractors and chaos suppression in an impulsive discrete economical supply and demand dynamical system. *Commun. Nonlinear Sci. Numer. Simul.* **2019**, *74*, 1–13.
21. Pham, V.-T.; Jafari, S.; Volos, C.; Kapitaniak, T. Different families of hidden attractors in a new chaotic system with variable equilibrium. *Int. J. Bifurc. Chaos* **2017**, *27*, 1750138. [[CrossRef](#)]
22. Jafari, S.; Sprott, J.C.; Nazarimehr, F. Recent new examples of hidden attractors. *Eur. Phys. J. Spec. Top.* **2015**, *224*, 1469–1476. [[CrossRef](#)]
23. Jafari, S.; Pham, V.-T.; Golpayegani, S.M.R.H.; Moghtadaei, M.; Kingni, S.T. The relationship between chaotic maps and some chaotic systems with hidden attractors. *Int. J. Bifurc. Chaos* **2016**, *26*, 1650211. [[CrossRef](#)]
24. Bao, B.C.; Li, H.Z.; Zhu, L.; Zhang, X.; Chen, M. Initial-switched boosting bifurcations in 2D hyperchaotic map. *Chaos* **2020**, *30*, 033107. [[CrossRef](#)]
25. Panahi, S.; Sprott, J.C.; Jafari, S. Two simplest quadratic chaotic maps without equilibrium. *Int. J. Bifurc. Chaos* **2018**, *28*, 1850144. [[CrossRef](#)]
26. Khennaoui, A.A.; Ouannas, A.; Boulaaras, S.; Pham, V.-T.; Azar, A.T. A fractional map with hidden attractors: Chaos and control. *Eur. Phys. J. Spec. Top.* **2020**, *229*, 1083–1093. [[CrossRef](#)]
27. Zhang, X.; Chen, G.R. Polynomial maps with hidden complex dynamics. *Discret. Contin. Dyn. Syst. Ser. B* **2019**, *24*, 2941–2954. [[CrossRef](#)]
28. Zambrano-Serrano, E.; Bekiros, S.; Platas-Garza, M.A.; Posadas-Castillo, C.; Agarwal, P.; Jahanshahi, H.; Aly, A.A. On chaos and projective synchronization of a fractional difference map with no equilibria using a fuzzy-based state feedback control. *Phys. A* **2021**, *578*, 126100. [[CrossRef](#)]
29. Liu, X.J.; Tang, D.F.; Hong, L. A fractional-order sinusoidal discrete map. *Entropy* **2022**, *24*, 320. [[CrossRef](#)]
30. Peng, Y.X.; Sun, K.H.; He, S.B. A discrete memristor model and its application in Hénon map. *Chaos Solitons Fractals* **2020**, *137*, 109873. [[CrossRef](#)]
31. Bao, H.; Hua, Z.Y.; Li, H.Z.; Chen, M.; Bao, B.C. Discrete memristor hyperchaotic maps. *IEEE Trans. Circuits Syst. I* **2021**, *68*, 4534–4544. [[CrossRef](#)]
32. Deng, Y.; Li, Y.X. Nonparametric bifurcation mechanism in 2-D hyperchaotic discrete memristor-based map. *Nonlinear Dyn.* **2021**, *104*, 4601–4614. [[CrossRef](#)]
33. Ma, M.L.; Yang, Y.; Qiu, Z.C.; Peng, Y.X.; Sun, Y.C.; Li, Z.J.; Wang, M.J. A locally active discrete memristor model and its application in a hyperchaotic map. *Nonlinear Dyn.* **2022**, *107*, 2935–2949. [[CrossRef](#)]
34. Lai, Q.; Lai, C. Design and implementation of a new hyperchaotic memristive map. *IEEE Trans. Circuits Syst. II* **2022**, *69*, 2331–2335. [[CrossRef](#)]
35. Fiori, S.; Di Filippo, R. An improved chaotic optimization algorithm applied to a DC electrical motor modeling. *Entropy* **2017**, *19*, 665. [[CrossRef](#)]
36. Zhang, X.; Wang, T.S.; Bao, H.; Hu, Y.H.; Bao, B.C. Stability effect of load converter on source converter in a cascaded buck converter. *IEEE Trans. Power Electron.* **2022**. [[CrossRef](#)]
37. Botella-Soler, V.; Castelo, J.M.; Oteo, J.A.; Ros, J. Bifurcations in the Lozi map. *J. Phys. A: Math. Theor.* **2011**, *44*, 305101. [[CrossRef](#)]
38. Bao, B.C.; Zhou, G.H.; Xu, J.P.; Liu, Z. Unified classification of operation-state regions for switching converters with ramp compensation. *IEEE Trans. Power Electron.* **2011**, *26*, 1968–1975. [[CrossRef](#)]
39. Pisarchik, A.N.; Feudel, U. Control of multistability. *Phys. Rep.* **2014**, *540*, 167–218. [[CrossRef](#)]
40. Bao, H.; Hua, Z.Y.; Li, H.Z.; Chen, M.; Bao, B.C. Memristor-based hyperchaotic maps and application in auxiliary classifier generative adversarial nets. *IEEE Trans. Ind. Inform.* **2022**, *18*, 5297–5306. [[CrossRef](#)]